Appendix of Finding Optimal Tangent Points for Reducing Distortions of Hard-label Attacks

Chen Ma [1] **Xiangyu Guo** [2] **Li Chen** [1,*] **Jun-Hai Yong** [1] **Yisen Wang** [3,4]
[1] School of Software, BNRist, Tsinghua University, Beijing, China
[2] Department of Computer Science and Engineering, University at Buffalo, Buffalo NY, USA
[3] Key Lab. of Machine Perception, School of Artificial Intelligence, Peking University, Beijing, China
[4] Institute for Artificial Intelligence, Peking University, Beijing, China
`machenstar@163.com`, `xiangyug@buffalo.edu`
`{chenlee,yongjh}@tsinghua.edu.cn`, `yisen.wang@pku.edu.cn`

A Potential Negative Societal Impacts

The adversarial attack is a major security concern in the real-world machine learning system, because the generated adversarial perturbation could be used for the malicious purpose. Our study relies only on the top-1 predicted label to craft the adversarial examples which is applicable to most real-world systems, making it more useful and practical. Although the experiments in this paper are about attacking the image classifier, this method can be used in other settings, such as the object detection, the recommender system, the facial recognition system, and the autonomous driving. In summary, this study could be used in harmful ways by malicious users.

In a broader perspective, the adversarial example is not restricted to malicious applications, and it can be used in the positive side, *e.g.,* the generation of CAPTCHA and the privacy protection. In particular, the study of adversarial attacks can promote the defense techniques. In recent years, many proposed defenses are broken by the latest attacks, which stimulates the development of defenses.

Our results also point to the potential defense techniques against hard-label attacks. For example, the defense can prohibit queries near the decision boundary, then the approximate gradient cannot be estimated, making Tangent Attack ineffective. Another possible defense is to add random perturbations to the input image to prevent effective gradient estimation, or predict random classification labels for samples near the classification decision boundary.

B Proof of Theorem 1

B.1 Notations and Assumption

Before we formally prove Theorem 1, let us first define the notations that will be used in the proof. Let $\mathbf{x}$ denote the original image, and w.l.o.g. we assume the boundary sample $\mathbf{x}_{t-1} = \mathbf{0}$ be the origin of the coordinate axis. Let B denote a n-dimensional ball centered at $\mathbf{x}_{t-1}$ with the radius of R, and its surface is denoted as $S := \partial B$. Note that B denotes a complete ball in this proof. However, B denotes the hemisphere in the main text of the paper. Theorem 1 assumes that the classification decision boundary of the target model is the hyperplane H, which is defined by its unit normal vector $\mathbf{u}$. Then, the hyperplane H divides $\mathbb{R}^n$ into two half-spaces:

$$\begin{aligned} H_{\geq 0} &= \{\mathbf{v} \in \mathbb{R}^n \mid \langle \mathbf{v}, \mathbf{u} \rangle \geq 0\}, \\ H_{\leq 0} &= \{\mathbf{v} \in \mathbb{R}^n \mid \langle \mathbf{v}, \mathbf{u} \rangle \leq 0\}. \end{aligned} \tag{1}$$

In the attack, $H_{\geq 0}$ mainly contains the adversarial region, and $H_{\leq 0}$ represents the non-adversarial region. In Fig. 1, we visually represent the hyperplane H and two half-spaces in $\mathbb{R}^3$. Suppose

[*] Corresponding author.

35th Conference on Neural Information Processing Systems (NeurIPS 2021).

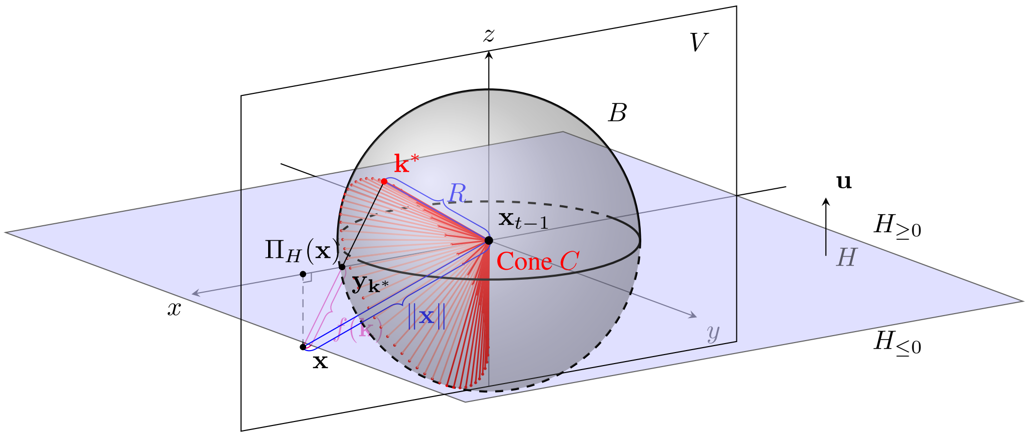

Figure 1: Illustration of the entities defined in the proof, where C is a convex cone whose boundary intersects with the circle formed by all the tangent points from $\mathbf{x}$ to the ball B.

$\mathbf{x} \in H_{\leq 0} \setminus B$ is a fixed point outside B such that $\langle \mathbf{x}, \mathbf{u} \rangle < 0$. Now, let us define the cosine function $\cos(\mathbf{a}, \mathbf{b}) := \frac{\langle \mathbf{a}, \mathbf{b} \rangle}{\|\mathbf{a}\| \|\mathbf{b}\|}$ to represent the cosine of the angle between two vectors, then we can define the convex cone C with $\mathbf{x}_{t-1}$ as its vertex, as shown below:

$$C := \left\{ \mathbf{v} \in \mathbb{R}^n \mid \cos(\mathbf{v}, \mathbf{x}) \geq \frac{R}{\|\mathbf{x}\|} \right\}. \tag{2}$$

Fig. 1 demonstrates the convex cone C in $\mathbb{R}^3$. For $\mathbf{v} \in S \cap C$ that satisfies $\cos(\mathbf{v}, \mathbf{x}) = R \,/\, \|\mathbf{x}\|$, the equation $\|\mathbf{v} - \mathbf{x}\|^2 = \|\mathbf{x}\|^2 - \|\mathbf{v}\|^2$ holds, *i.e.,* $\mathbf{v}$ is the tangent point of the tangent line from $\mathbf{x}$ to the surface of B.

To make the feasible region of the optimization problem (3) in Theorem 1 nonempty, we need to make an assumption about the positional relationship between $\mathbf{x}$ and the ball B. Let $\Pi_H : \mathbb{R}^n \mapsto H$ denote the orthogonal projection from $\mathbb{R}^n$ onto the hyperplane H, we make the following assumption:

Assumption B.1. $\Pi_H(\mathbf{x}) \in C$

Note that Assumption B.1 is not really an "assumption": it essentially means that there is a tangent point on $S \cap H_{\geq 0}$, which is in the adversarial region. Assumption B.1 means the feasible region of the optimization problem (3) is a nonempty set. By repeatedly reducing the radius R, the algorithm guarantees that the optimal tangent point is in the adversarial region, thereby making Assumption B.1 always hold. In addition, according to Assumption B.1, $\|\Pi_H(\mathbf{x})\| \geq R$ holds.

In Theorem 1, $\mathbf{k}$ is an arbitrary point on the surface of the hemisphere $B \cap H_{\geq 0}$, so this proof mainly focuses on points in this region. In the following text, the hemisphere is denoted as $B' := B \cap H_{\geq 0}$, and its surface is denoted as $S' := S \cap H_{\geq 0}$ for brevity. Now, let us pick up any $\mathbf{k} \in S'$[2], and then the intersection point between the hyperplane H and the line passing through $\mathbf{x}$ and $\mathbf{k}$ is denoted as $\mathbf{y}_\mathbf{k}$. Then, $(\mathbf{y}_\mathbf{k}, \lambda)$ is the unique solution of the following equation system:

$$\begin{aligned} &\mathbf{y}_\mathbf{k} = \lambda \mathbf{k} + (1 - \lambda)\mathbf{x}, \\ &\langle \mathbf{y}_\mathbf{k}, \mathbf{u} \rangle = 0, \\ &0 \leq \lambda \leq 1. \end{aligned} \tag{3}$$

Because the position of $\mathbf{k}$ determines the distance between $\mathbf{y}_\mathbf{k}$ and $\mathbf{x}$, we can define the function $f(\mathbf{k}) := \|\mathbf{y}_\mathbf{k} - \mathbf{x}\|$ to represent the distance between $\mathbf{x}$ and $\mathbf{y}_\mathbf{k}$.

B.2 Proof

To prove Theorem 1, we turn to prove the following lemma, which is equivalent to Theorem 1.

[2] Note that $\mathbf{k}$ defined here may not be a tangent point on the ball.

Lemma 1. *Let S', f be defined as above, then minimizing f over the feasible region S' is equivalent to finding the point* $\mathbf{k}$ *from the set $S' \cap C$ that is farthest away from H, i.e.,*

$$\arg\min_{\mathbf{k}\in S'} f(\mathbf{k}) = \arg\max_{\mathbf{k}\in(S'\cap C)} \langle \mathbf{k}, \mathbf{u}\rangle. \tag{4}$$

In addition, we can replace S' with B' in the above equation, and the optimal solution of $f(\mathbf{k})$ does not change. In other words, when the feasible region is B', the optimal solution can be always obtained at the surface of B'. Thus, the following equation holds:

$$\arg\min_{\mathbf{k}\in S'} f(\mathbf{k}) = \arg\min_{\mathbf{k}\in B'} f(\mathbf{k}) = \arg\max_{\mathbf{k}\in(S'\cap C)} \langle \mathbf{k}, \mathbf{u}\rangle = \arg\max_{\mathbf{k}\in(B'\cap C)} \langle \mathbf{k}, \mathbf{u}\rangle. \tag{5}$$

Proof. By simplifying the original problem to a two-dimensional plane, the proof of Lemma 1 will be readily apparent. Let $V := \mathrm{span}(\{\mathbf{x}, \mathbf{u}\})$ be the plane spanned by $\mathbf{x}$ and $\mathbf{u}$. It is easy to observe B, S, C, B', and S' are symmetrical about the plane V. Next, we will show that for any $\mathbf{k} \in B'$, there must exist a point $\mathbf{k}^* \in S' \cap V$ such that $f(\mathbf{k}^*) \le f(\mathbf{k})$. To find the $\mathbf{k}^*$ that satisfies the condition, we introduce the notation $\Pi_V : \mathbb{R}^n \mapsto V$ to denote the projection from $\mathbb{R}^n$ to V.

Now, take any $\mathbf{k} \in B'$, and use $\mathbf{k}''$ to denote the mirror point of $\mathbf{k}$ with respect to V, as shown in Fig. 2. The projection point $\Pi_V(\mathbf{k})$ is the midpoint of the line between $\mathbf{k}$ and $\mathbf{k}''$, *i.e.,* $\mathbf{k}'' = 2\Pi_V(\mathbf{k}) - \mathbf{k}$. Note that if $\mathbf{k} \in V$, then $\mathbf{k}$, $\mathbf{k}'$ and $\mathbf{k}''$ coincide. Since B' is symmetrical about the plane V, we have $\mathbf{k}'' \in B'$. Now since B' is the intersection of two convex sets B and $H_{\ge 0}$, we know that B' is also a convex set. Notice that $\Pi_V(\mathbf{k}) = \frac{1}{2} \cdot (\mathbf{k} + \mathbf{k}'')$ is a convex combination of $\mathbf{k}$ and $\mathbf{k}''$, and B' is a convex set, thus we conclude $\Pi_V(\mathbf{k}) \in B'$.

Now, we will show that we can ignore any point outside of V, thus restricting the problem to the two-dimensional plane V. Formally, the following inequality holds for any $\mathbf{k}$:

$$f\left(\Pi_V(\mathbf{k})\right) \le f(\mathbf{k}). \tag{6}$$

The above inequality is easy to prove. Because $\mathbf{x} \in V$, we have $\|\Pi_V(\mathbf{y_k} - \mathbf{x})\| = \|\Pi_V(\mathbf{y_k}) - \mathbf{x}\|$. Therefore,

$$f\left(\Pi_V(\mathbf{k})\right) = \|\Pi_V(\mathbf{y_k}) - \mathbf{x}\| = \|\Pi_V(\mathbf{y_k} - \mathbf{x})\| \le \|\mathbf{y_k} - \mathbf{x}\| = f(\mathbf{k}). \tag{7}$$

Now, we can focus on the plane V and find the optimal $\mathbf{k}^*$ on it such that $f(\mathbf{k}^*) \le f\left(\Pi_V(\mathbf{k})\right)$. Let us define C_0 to denote the convex cone with the point $\mathbf{x}$ as the vertex, and its boundary is formed by all tangent lines from $\mathbf{x}$ to B:

$$C_0 := \left\{ \mathbf{v} \in \mathbb{R}^n \mid \cos(\mathbf{v} - \mathbf{x}, -\mathbf{x}) \ge \sqrt{1 - \frac{R^2}{\|\mathbf{x}\|^2}} \right\}. \tag{8}$$

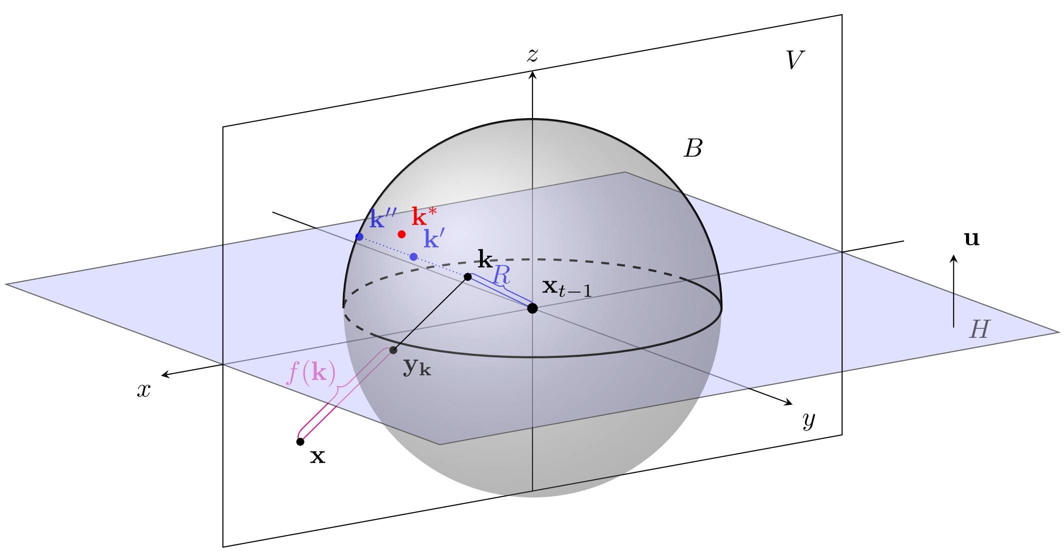

Figure 2: Illustration of the points used in proving Lemma 1, where $\mathbf{k}''$ is the mirror point of $\mathbf{k}$ with respect to the plane V, and $\mathbf{k}'$ is the projection of $\mathbf{k}$ onto the plane V.

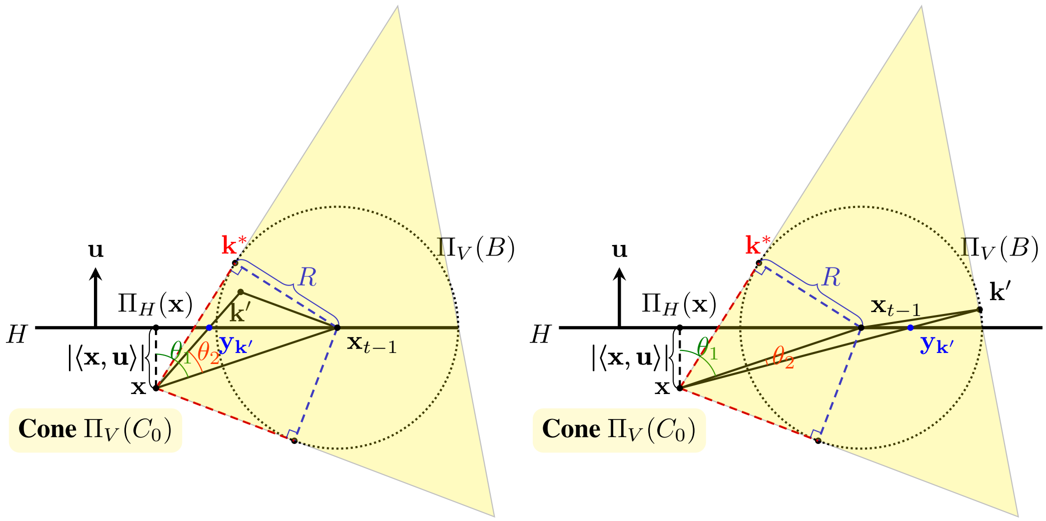

(a) $\mathbf{y}_{\mathbf{k}'}$ and $\Pi_H(\mathbf{x})$ are on the same side of $\mathbf{x}_{t-1}$. (b) $\mathbf{y}_{\mathbf{k}'}$ and $\Pi_H(\mathbf{x})$ are on different sides of $\mathbf{x}_{t-1}$.

Figure 3: Illustration of the problem reduced to the plane V.

Let $\mathbf{k}' := \Pi_V(\mathbf{k})$ be the projection point of $\mathbf{k}$ onto the plane V (see Fig. 3). Because $\mathbf{k}' \in B'$ and $\mathbf{k}' \in V$, we have $\mathbf{k}' \in \Pi_V(B')$. Now, we define $\mathbf{k}^* \in S' \cap C_0 \cap V$ to be the tangent point from $\mathbf{x}$ to the semicircle $\Pi_V(B')$. We claim $\mathbf{k}^*$ is the optimal one that attains the minimum $f(\mathbf{k}')$ among all $\mathbf{k}'$ in $\Pi_V(B')$. We denote the angle between $-\mathbf{x}$ and $\mathbf{u}$ as θ_1, *i.e.,* $\theta_1 := \arccos(\cos(-\mathbf{x}, \mathbf{u}))$. The angle between $-\mathbf{x}$ and $\mathbf{k}' - \mathbf{x}$ is denoted as θ_2, *i.e.,* $\theta_2 := \arccos(\cos(-\mathbf{x}, \mathbf{k}' - \mathbf{x}))$. Based on the position of $\mathbf{k}'$ in $\Pi_V(B')$, there are two possible cases for the angle θ_2, as shown in Fig. 3a and Fig. 3b, respectively. We discuss them separately below.

In the first case (Fig. 3a), $\mathbf{y}_{\mathbf{k}'}$ and $\Pi_H(\mathbf{x})$ are on the same side of $\mathbf{x}_{t-1}$. By Assumption B.1, we know that $\|\Pi_H(\mathbf{x})\| \geq R$, so $\cos(-\mathbf{x}, \mathbf{u}) = \sqrt{1 - \|\Pi_H(\mathbf{x})\|^2 / \|\mathbf{x}\|^2} \leq \sqrt{1 - R^2 / \|\mathbf{x}\|^2}$. According to the definition of the convex cone C_0, $\mathbf{u}$ is outside C_0. Notice that $\mathbf{x} \in C_0$ and $\mathbf{k}' \in \Pi_V(B')$, hence $\mathbf{k}' - \mathbf{x}$ is in the convex cone $\Pi_V(C_0)$. Therefore, based on the positions of the two vectors $\mathbf{u}$ and $\mathbf{k}' - \mathbf{x}$ with respect to the cone $\Pi_V(C_0)$, we conclude that $\theta_1 \geq \theta_2$. In such case, the distance function is $f(\mathbf{k}') = \|\mathbf{y}_{\mathbf{k}'} - \mathbf{x}\| = |\langle \mathbf{x}, \mathbf{u}\rangle| / \cos(\theta_1 - \theta_2)$, as shown in Fig. 3a. Because both $\mathbf{x}$ and $\mathbf{u}$ are fixed, the value of θ_1 is fixed. Therefore, the only way to minimize $f(\mathbf{k}')$ is to maximize θ_2. Among all possible choices of $\mathbf{k}'$ in $\Pi_V(B')$, the $\mathbf{k}'$ that maximizes the angle θ_2 appears on the boundary of $\Pi_V(C_0) \cap H_{\geq 0}$. The only point that satisfies this condition is the tangent point $\mathbf{k}^*$. Therefore, in the first case, $\arg\min_{\mathbf{k}\in B'} f(\mathbf{k}) = \mathbf{k}^*$.

In the second case (Fig. 3b), $\mathbf{y}_{\mathbf{k}'}$ and $\Pi_H(\mathbf{x})$ are on different sides of $\mathbf{x}_{t-1}$. In this case, $\theta_2 \geq 0$. In particular, when $\theta_2 = 0$, $\mathbf{y}_{\mathbf{k}'}$ and $\mathbf{x}_{t-1}$ coincide. According to Assumption B.1, $\theta_1 > 0$. The distance function can be defined as $f(\mathbf{k}') = \|\mathbf{y}_{\mathbf{k}'} - \mathbf{x}\| = |\langle \mathbf{x}, \mathbf{u}\rangle| / \cos(\theta_1 + \theta_2)$ in this case. Because $\theta_1 > 0$ and $\theta_2 \geq 0$, the following inequality holds:

$$f(\mathbf{k}') = \frac{|\langle \mathbf{x}, \mathbf{u}\rangle|}{\cos(\theta_1 + \theta_2)} \geq \frac{|\langle \mathbf{x}, \mathbf{u}\rangle|}{\cos(\theta_1)} \geq \frac{|\langle \mathbf{x}, \mathbf{u}\rangle|}{\cos(\theta_1 - \theta_2)}. \tag{9}$$

According to the above inequality, the distance obtained from the second case is greater than or equal to the distance in the first case, and the distances in both cases are equal only if $\theta_2 = 0$. Therefore, we can still conclude that $f(\mathbf{k}') \geq f(\mathbf{k}^*)$, *i.e.,* $\arg\min_{\mathbf{k}\in B'} f(\mathbf{k}) = \mathbf{k}^*$.

Finally, we need to prove $\arg\max_{\mathbf{k}\in(B'\cap C)} \langle \mathbf{k}, \mathbf{u}\rangle = \mathbf{k}^*$, so that Eq. (5) holds. The overall proof process is similar to the above proof, except that all $f(\mathbf{k})$ in the above proof need to be replaced by $\langle \mathbf{k}, \mathbf{u}\rangle$. Correspondingly, Eq. (6) needs to be changed to the following formula:

$$\langle \mathbf{k}^*, \mathbf{u}\rangle \geq \langle \Pi_V(\mathbf{k}), \mathbf{u}\rangle = \langle \mathbf{k}, \mathbf{u}\rangle. \tag{10}$$

Firstly, let us prove the equality part of Eq. (10): when projecting any $\mathbf{k} \in (B' \cap C)$ onto the plane V, the value of $\langle \mathbf{k}, \mathbf{u}\rangle$ does not change. Thus, we have $\langle \Pi_V(\mathbf{k}), \mathbf{u}\rangle = \langle \mathbf{k}, \mathbf{u}\rangle$. Secondly, we prove the inequality part of Eq. (10): $\langle \mathbf{k}^*, \mathbf{u}\rangle \geq \langle \Pi_V(\mathbf{k}), \mathbf{u}\rangle$. Now the problem is reduced to the plane V again.

Because $\Pi_V(\mathbf{k}) \in (B' \cap C \cap V)$, only the first case mentioned above can happen (Fig. 3a). By a similar argument, we conclude that $\arg\max_{\mathbf{k}\in(B'\cap C)} \langle \mathbf{k}, \mathbf{u} \rangle = \mathbf{k}^*$ holds, which proves Lemma 1. Consequently, Theorem 1 holds. $\square$

C Experimental Settings

In this section, we provide the hyperparameter settings of the compared methods, *i.e.,* HopSkipJumpAttack (HSJA) [2], Boundary Attack (BA) [1], Sign-OPT [3], and SVM-OPT [3]. In addition, the proposed Tangent Attack is abbreviated as TA, and the Generalized Tangent Attack is abbreviated as G-TA.

Table 1: The hyperparameters of HSJA.

Dataset	Hyperparameter	Value
CIFAR-10	γ, threshold of the binary search	1.0
	B_0, the initial batch size for gradient estimation	100
	B_{max}, the maximum batch size for gradient estimation	10,000
	the search method for step size	geometric progression
	number of iterations	64
ImageNet	γ, threshold of the binary search	1,000.0
	B_0, the initial batch size for gradient estimation	100
	B_{max}, the maximum batch size for gradient estimation	10,000
	the search method for step size	geometric progression
	number of iterations	64

Table 2: The hyperparameters of BA.

Hyperparameter	Value
maximum number of trials per iteration	25
number of iterations	1,200
spherical step size	0.01
source step size	0.01
step size adaptation multiplier	1.5
disable automatic batch size tuning	False
generate candidates and random numbers without using multithreading	False

Table 3: The hyperparameters of Sign-OPT.

Hyperparameter	Value
k, number of queries for estimating an approximate gradient	200
α, the update step size of the direction θ	0.2
β, used for the gradient estimation of θ and determining the stopping threshold of binary search	0.001
the number of iterations	1,000
the binary search's stopping threshold of the CIFAR-10 dataset	$\frac{\beta}{500}$
the binary search's stopping threshold of the ImageNet dataset	1×10^{-4}

Experimental Equipment. The experiments of all compared methods are conducted by using PyTorch 1.7.1 framework on a NVIDIA 1080Ti GPU.

HSJA. Hyperparameters of HSJA [2] are listed in Table 1. We translate the implementation code into the PyTorch version for the experiments. In the experiments of targeted attacks, we randomly select an image from the target class as the initial adversarial example. For fair comparison, we set the hyperparameters of TA and G-TA to be the same with HSJA, *i.e.,* the same initial batch size B_0 and the same γ.

BA. Hyperparameters of BA [1] are listed in Table 2. In the experiments, we directly use the implementation of BA from Foolbox 2.0 [8, 9], and adopt a randomly selected image from the target class as the initialization in the targeted attack.

Table 4: The hyperparameters of SVM-OPT.

Hyperparameter	Value
k, number of queries for estimating gradients	100
α, the step size of the gradient descent of θ	0.2
β, used for the gradient estimation of θ and determining the stopping threshold of binary search	0.001
the number of iterations	1,000
the binary search's stopping threshold of the CIFAR-10 dataset	$\frac{\beta}{500}$
the binary search's stopping threshold of the ImageNet dataset	1×10^{-4}

Sign-OPT and SVM-OPT. Hyperparameters of Sign-OPT [3] and SVM-OPT [3] are listed in Tables 3 and 4. We translate the implementation code into the PyTorch version for the experiments. In the experiments of targeted attacks, we set the initial direction θ_0 of Sign-OPT and SVM-OPT to the direction of a randomly selected image of the target class.

D Experimental Results

D.1 Limitation of Tangent Attack

The proposed approach supports all types of attacks, including both untargeted and targeted attacks under the both ℓ_2 and ℓ_∞ norm constraints. This is the strength of the proposed approach. However, in the ℓ_∞ norm attack, TA and G-TA obtain the similar performance to the baseline method HSJA. Because under the definition of the ℓ_∞ norm distance: $D_{\ell_\infty}(x,y) := \max_i(|x_i - y_i|), i \in \{1,\dots,d\}$ (d is the image dimension), the intersection of the tangent line and the decision boundary may not be the one with the shortest ℓ_∞ norm distance to the original image. Therefore, searching the boundary sample along the tangent line cannot always outperform HSJA in the ℓ_∞ norm attack.

Tables 5 and 6 demonstrate the experimental results of attacking against undefended models on the CIFAR-10 and ImageNet datasets.

Table 5: Mean ℓ_∞ distortions of different query budgets on the ImageNet dataset, where the radius ratio r is set to 1.1 in G-TA. BA is not applicable to the ℓ_∞ norm attack, hence it is not listed.

Target Model	Method	Targeted Attack						Untargeted Attack					
		@300	@1K	@2K	@5K	@8K	@10K	@300	@1K	@2K	@5K	@8K	@10K
Inception-v3	Sign-OPT [3]	0.557	0.519	0.481	0.421	0.390	0.375	1.078	0.792	0.548	0.328	0.262	0.239
	SVM-OPT [3]	0.558	0.512	0.476	0.423	0.397	0.385	1.079	0.763	0.526	0.336	0.280	0.260
	HSJA [2]	0.370	0.330	**0.289**	**0.211**	**0.169**	**0.147**	0.305	0.236	0.174	**0.093**	0.069	**0.059**
	TA	0.370	0.330	0.291	0.216	0.172	0.149	**0.304**	**0.234**	**0.173**	**0.093**	**0.068**	**0.059**
	G-TA	**0.364**	**0.326**	**0.289**	0.220	0.179	0.159	**0.304**	0.238	0.174	**0.093**	**0.068**	**0.059**
Inception-v4	Sign-OPT [3]	0.545	0.504	0.464	0.402	0.370	0.355	1.176	0.867	0.603	0.369	0.296	0.270
	SVM-OPT [3]	0.547	0.498	0.460	0.406	0.379	0.367	1.181	0.842	0.588	0.381	0.319	0.296
	HSJA [2]	0.357	**0.324**	**0.287**	**0.215**	**0.175**	**0.152**	**0.336**	**0.257**	**0.185**	**0.091**	**0.060**	**0.048**
	TA	**0.354**	0.328	0.294	0.221	0.182	0.161	0.337	0.264	0.196	0.103	0.073	0.062
	G-TA	**0.354**	**0.324**	0.290	0.220	0.182	0.162	0.337	0.264	0.196	0.104	0.073	0.061
SENet-154	Sign-OPT [3]	0.537	0.491	0.439	0.357	0.316	0.298	0.806	0.631	0.462	0.299	0.247	0.227
	SVM-OPT [3]	0.538	0.480	0.429	0.357	0.322	0.307	0.807	0.608	0.444	0.306	0.262	0.246
	HSJA [2]	0.347	**0.288**	**0.249**	**0.176**	**0.139**	**0.119**	**0.253**	**0.195**	**0.141**	0.071	0.048	0.039
	TA	0.346	0.289	0.251	0.181	0.142	0.123	**0.253**	0.196	**0.141**	0.071	**0.047**	**0.038**
	G-TA	**0.344**	**0.288**	0.252	0.179	0.142	0.123	**0.253**	0.196	**0.141**	**0.070**	**0.047**	**0.038**
ResNet-101	Sign-OPT [3]	0.549	0.501	0.450	0.370	0.329	0.309	0.645	0.515	0.385	0.251	0.206	0.190
	SVM-OPT [3]	0.550	0.492	0.444	0.371	0.335	0.319	0.642	0.494	0.370	0.258	0.220	0.206
	HSJA [2]	0.340	0.283	0.247	**0.179**	**0.143**	**0.125**	0.197	**0.140**	**0.098**	**0.049**	**0.034**	**0.028**
	TA	0.340	0.282	**0.246**	0.180	**0.143**	**0.125**	**0.196**	0.145	0.109	0.064	0.050	0.044
	G-TA	**0.337**	**0.280**	**0.246**	0.182	0.150	0.132	**0.196**	0.147	0.110	0.064	0.050	0.044

The results of Tables 5 and 6 show that HSJA, TA and G-TA obtain the similar average ℓ_∞ distortions. Therefore, although the proposed approach is applicable to ℓ_∞ norm attack, the performance is similar to that of the baseline method HSJA.

Table 6: Mean ℓ_∞ distortions of different query budgets on the CIFAR-10 dataset, where the radius ratio r is set to 1.5 in G-TA. BA is not applicable to the ℓ_∞ norm attack, and thus it is not listed.

Target Model	Method	Targeted Attack						Untargeted Attack					
		@300	@1K	@2K	@5K	@8K	@10K	@300	@1K	@2K	@5K	@8K	@10K
PyramidNet-272	Sign-OPT [3]	0.395	0.318	0.237	0.134	0.096	0.082	0.284	0.189	0.115	0.059	0.047	0.043
	SVM-OPT [3]	0.390	0.299	0.226	0.134	0.099	0.087	0.286	0.173	0.104	0.059	0.049	0.046
	HSJA [2]	**0.218**	0.155	**0.112**	**0.057**	**0.039**	0.032	**0.133**	**0.056**	**0.034**	**0.016**	**0.012**	0.011
	TA	0.219	0.154	**0.112**	**0.057**	**0.039**	0.032	0.134	0.057	0.035	0.017	0.013	0.011
	G-TA	**0.218**	**0.153**	0.113	**0.057**	**0.039**	**0.031**	**0.133**	**0.056**	**0.034**	**0.016**	**0.012**	**0.010**
GDAS	Sign-OPT [3]	0.398	0.332	0.266	0.153	0.107	0.089	0.305	0.269	0.231	0.185	0.167	0.160
	SVM-OPT [3]	0.389	0.325	0.267	0.164	0.118	0.100	0.304	0.257	0.219	0.181	0.168	0.163
	HSJA [2]	**0.210**	**0.147**	**0.112**	**0.060**	**0.040**	**0.031**	**0.049**	**0.029**	**0.020**	**0.011**	**0.009**	**0.008**
	TA	0.214	0.151	0.115	0.062	0.041	0.032	**0.049**	**0.029**	**0.020**	**0.011**	**0.009**	**0.008**
	G-TA	0.214	0.151	0.116	0.062	0.041	0.032	**0.049**	**0.029**	**0.020**	**0.011**	**0.009**	**0.008**
WRN-28	Sign-OPT [3]	0.402	0.307	0.225	0.121	0.086	0.074	0.200	0.130	0.085	0.053	0.044	0.041
	SVM-OPT [3]	0.382	0.296	0.223	0.128	0.093	0.080	0.201	0.121	0.079	0.052	0.045	0.043
	HSJA [2]	**0.185**	**0.106**	0.070	0.032	**0.021**	**0.018**	**0.090**	0.031	**0.020**	**0.012**	**0.010**	**0.009**
	TA	0.186	0.107	0.070	**0.031**	**0.021**	**0.018**	**0.090**	**0.030**	**0.020**	**0.012**	**0.010**	**0.009**
	G-TA	**0.185**	**0.106**	**0.069**	0.032	0.022	**0.018**	**0.090**	**0.030**	**0.020**	**0.012**	**0.010**	**0.009**
WRN-40	Sign-OPT [3]	0.397	0.305	0.220	0.120	0.085	0.073	0.284	0.208	0.125	0.051	0.042	0.039
	SVM-OPT [3]	0.381	0.293	0.220	0.126	0.092	0.079	0.273	0.190	0.120	0.057	0.045	0.041
	HSJA [2]	**0.194**	0.111	**0.072**	**0.032**	**0.022**	**0.019**	0.084	0.030	**0.020**	**0.012**	**0.010**	**0.009**
	TA	0.195	0.112	0.073	**0.032**	**0.022**	**0.019**	**0.082**	**0.029**	**0.020**	**0.012**	**0.010**	**0.009**
	G-TA	**0.194**	**0.110**	**0.072**	**0.032**	**0.022**	**0.019**	**0.082**	**0.029**	**0.020**	**0.012**	**0.010**	**0.009**

D.2 Experimental Results of Attacks against Defense Models

We also conduct experiments by using ℓ_∞ norm attacks to break five defense models, and the experimental results are shown in Table 7. The conclusion drawn from this table is the same as that in Tables 5 and 6: TA and G-TA obtain the similar performance with HSJA in ℓ_∞ norm attacks.

Table 7: The experimental results of performing ℓ_∞ norm attacks against the defense models on the CIFAR-10 dataset, where the radius ratio r is set to 1.5 in G-TA.

Target Model	Method	Untargeted Attack					
		@300	@1K	@2K	@5K	@8K	@10K
AT [7]	Sign-OPT [3]	0.731	0.519	0.395	0.288	0.255	0.243
	SVM-OPT [3]	0.719	0.498	0.382	0.287	0.261	0.251
	HSJA [2]	**0.181**	**0.145**	**0.121**	**0.090**	0.080	**0.075**
	TA	0.184	0.147	**0.121**	**0.090**	**0.079**	**0.075**
	G-TA	**0.181**	**0.145**	**0.121**	**0.090**	0.080	**0.075**
TRADES [11]	Sign-OPT [3]	0.748	0.562	0.419	0.304	0.269	0.257
	SVM-OPT [3]	0.743	0.534	0.409	0.308	0.281	0.271
	HSJA [2]	**0.194**	**0.162**	**0.137**	**0.106**	**0.095**	**0.090**
	TA	0.195	0.163	0.138	0.107	**0.095**	**0.090**
	G-TA	**0.194**	0.163	0.138	0.107	**0.095**	**0.090**
JPEG [4]	Sign-OPT [3]	0.301	0.292	0.281	0.262	0.250	0.245
	SVM-OPT [3]	0.301	0.288	0.275	0.256	0.249	0.246
	HSJA [2]	0.094	**0.086**	**0.078**	**0.066**	**0.061**	**0.058**
	TA	**0.093**	0.087	0.080	0.067	**0.061**	**0.058**
	G-TA	0.097	0.091	0.081	0.068	0.062	0.059
Feature Distillation [6]	Sign-OPT [3]	0.344	0.330	0.317	0.290	0.273	0.266
	SVM-OPT [3]	0.354	0.338	0.323	0.297	0.284	0.279
	HSJA [2]	0.090	0.087	0.080	0.069	0.064	0.061
	TA	**0.089**	**0.086**	**0.079**	0.070	0.063	0.060
	G-TA	0.090	**0.086**	**0.079**	**0.067**	**0.062**	**0.059**
Feature Scatter [10]	Sign-OPT [3]	0.561	0.380	0.246	0.135	0.110	0.101
	SVM-OPT [3]	0.550	0.344	0.222	0.137	0.116	0.110
	HSJA [2]	**0.202**	**0.137**	**0.104**	**0.062**	**0.048**	**0.042**
	TA	**0.202**	**0.137**	**0.104**	**0.062**	**0.048**	**0.042**
	G-TA	0.205	0.139	0.105	**0.062**	**0.048**	**0.042**

Next, we conduct experiments by using ℓ_2 norm attack to break different defense models on the CIFAR-10 and ImageNet datasets. In the CIFAR-10 dataset, we select six types of defense models:

- Adversarial Training (AT) [7]: the most effective defense method, which uses adversarial examples as the training data to obtain the robust classifier.
- TRADES [11]: an improved AT that optimizes a regularized surrogate loss.
- JPEG [4]: a standard image compression algorithm based on the discrete cosine transform, which can remove the adversarial perturbations, thereby providing some degree of defense.

- Feature Distillation [6]: a defense method based on the improved JPEG image compression. Its defense mechanism is divided into two steps. Firstly, it filters out adversarial perturbations by using a semi-analytical method. Secondly, it restores the classification accuracy of benign images by using a DNN-oriented quantization process.

- Feature Scatter [10]: a feature scattering-based AT method, which is an unsupervised approach for generating adversarial examples during the training.

- ComDefend [5]: a defense model that consists of a compression CNN and a reconstruction CNN to transform the adversarial image into its clean version to defend against attacks.

In the ImageNet dataset, we directly use the publicly available AT models for experiments, all of which use the ResNet-50 networks as their backbones. The pre-trained weights can be downloaded from `https://github.com/MadryLab/robustness`. In the experiments, we set the radius ratio r of G-TA to 1.5, and the experimental results are shown in Fig. 4. In untargeted attacks (Figs. 4a, 4b, 4c), the G-TA (the semi-ellipsoid version) outperforms the TA (the hemisphere version), and the baseline method HSJA outperforms TA and G-TA. We conjecture that it is because the classification decision boundaries of the AT models on the ImageNet dataset are extremely curved in untargeted attacks, resulting in the better performance of HSJA. In targeted attacks (Figs. 4d, 4e, 4f), both TA and G-TA outperform HSJA in the attacks of different AT models. These results indicate that TA and G-TA are more suitable for the targeted attack. Another interesting finding is that SVM-OPT performs better in untargeted attacks while Sign-OPT performs better in targeted attacks. We will explore the reasons for these results in the future work.

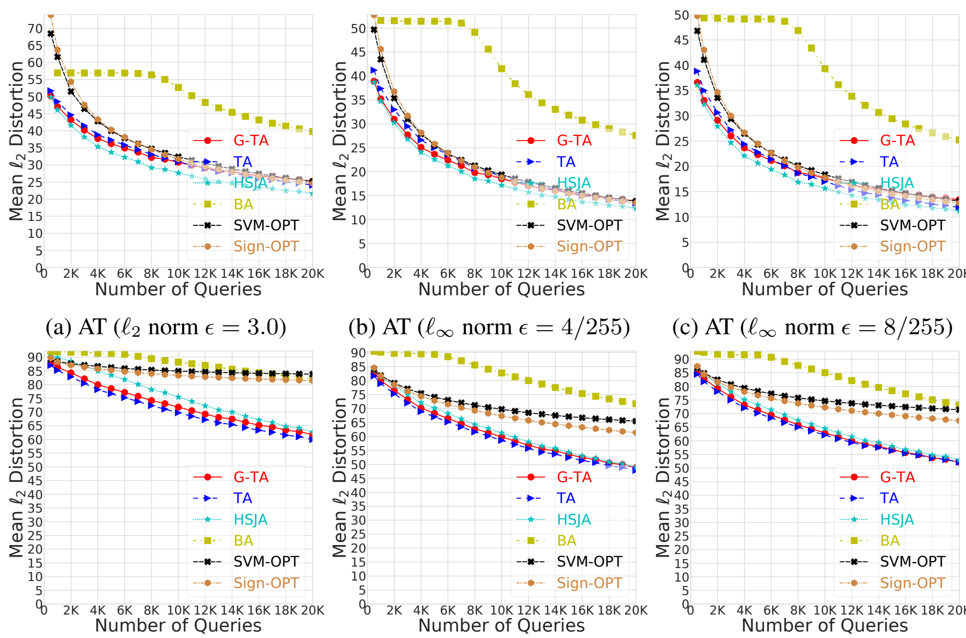

(a) AT (ℓ_2 norm $\epsilon = 3.0$) (b) AT (ℓ_∞ norm $\epsilon = 4/255$) (c) AT (ℓ_∞ norm $\epsilon = 8/255$)

(d) AT (ℓ_2 norm $\epsilon = 3.0$) (e) AT (ℓ_∞ norm $\epsilon = 4/255$) (f) AT (ℓ_∞ norm $\epsilon = 8/255$)

Figure 4: Experimental results of ℓ_2 norm attacks against adversarial trained ResNet-50 networks on the ImageNet dataset, where the first row (Figs. 4a, 4b, 4c) shows the results of untargeted attacks, and the second row (Figs. 4d, 4e, 4f) shows the results of targeted attacks.

Figs. 5 and 6 show the experimental results of untargeted and targeted attacks on the CIFAR-10 dataset, respectively. In the results of untargeted attacks (Fig. 5), G-TA outperforms HSJA and TA in the attacks of ComDefend, JPEG and Feature Distillation. When the target models are AT, Feature Scatter and TRADES, the performance of G-TA is similar to that of the baseline attack method HSJA.

In addition, in the experimental results of targeted attacks (Fig. 6), the performance of G-TA is similar to that of TA when attacking different defense models.

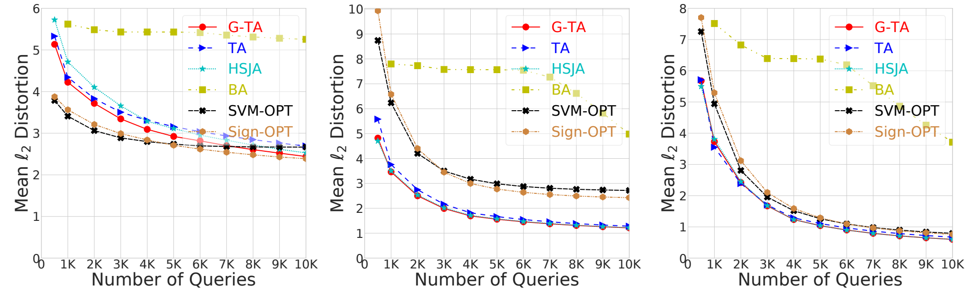

(a) ComDefend (b) AT (PGD-10 $\epsilon = 8/255$) (c) Feature Scatter

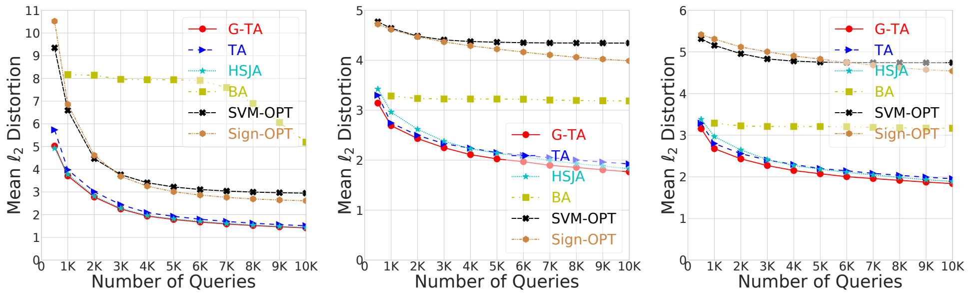

(d) TRADES ($\epsilon = 8/255$) (e) JPEG (f) Feature Distillation

Figure 5: Experimental results of the ℓ_2 norm untargeted attacks against defense models on the CIFAR-10 dataset, where all defense models adopt the backbone of ResNet-50 network.

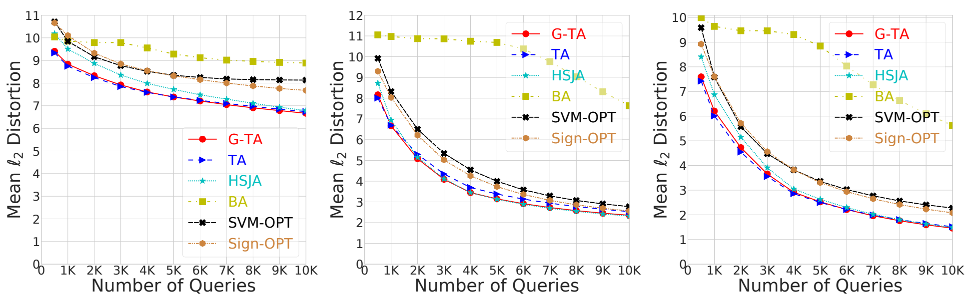

(a) ComDefend (b) AT (PGD-10 $\epsilon = 8/255$) (c) Feature Scatter

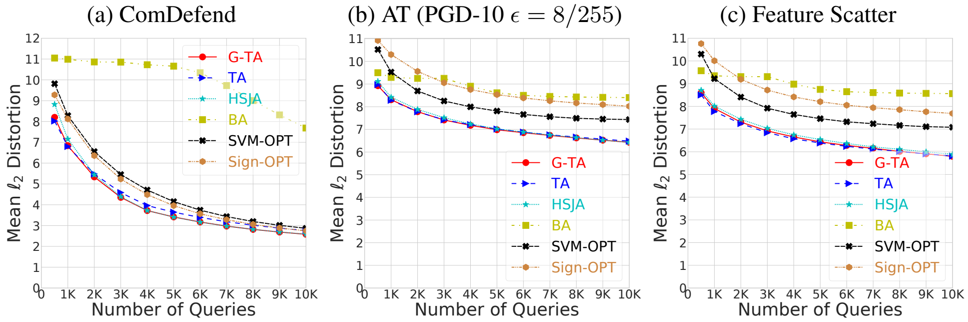

(d) TRADES ($\epsilon = 8/255$) (e) JPEG (f) Feature Distillation

Figure 6: Experimental results of the ℓ_2 norm targeted attacks against defense models on the CIFAR-10 dataset, where all defense models adopt the backbone of ResNet-50 network.

D.3 Distributions of Distortions across Different Adversarial Examples

So far, all the experimental results only show the average ℓ_2 distortion of $1{,}000$ adversarial examples. To check the distortion of each adversarial example in more detail, we extract the ℓ_2 distortions of 20 samples from HSJA, TA and G-TA. These samples are selected from $1{,}000$ images in the following way: from the 1st image to the $1{,}000$th image, we select one image for every 50 images. Fig. 7 shows the distributions of ℓ_2 distortions across 20 adversarial examples on the ImageNet dataset, where the

1st image's "image number index" is 0. The results indicate that the ℓ_2 distortions obtained by TA and G-TA are uniformly better than that of the baseline method HSJA. Thus, our approach can obtain better ℓ_2 distortions on different adversarial examples, not just on specific samples.

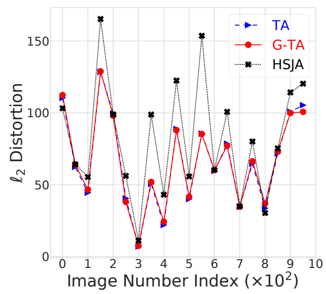

(a) Inception-v3 (query: 1K)

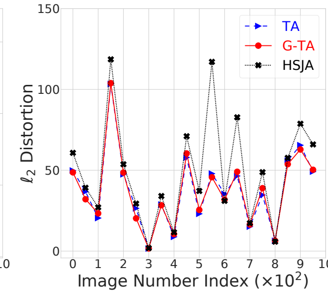

(b) Inception-v3 (query: 5K)

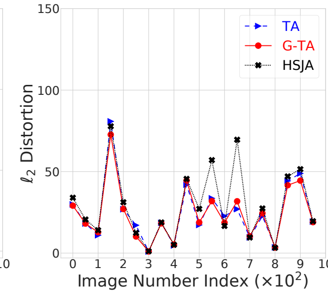

(c) Inception-v3 (query: 10K)

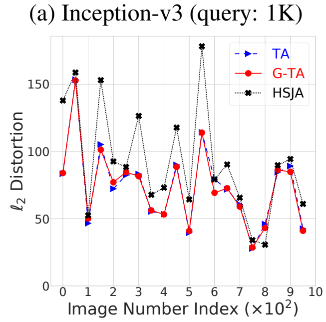

(d) Inception-v4 (query: 1K)

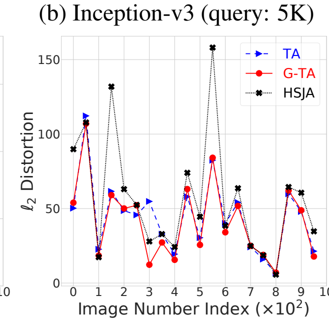

(e) Inception-v4 (query: 5K)

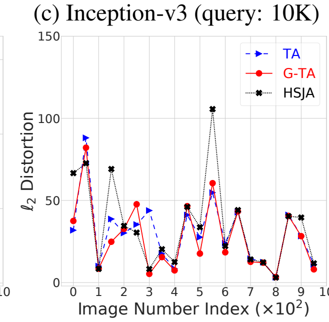

(f) Inception-v4 (query: 10K)

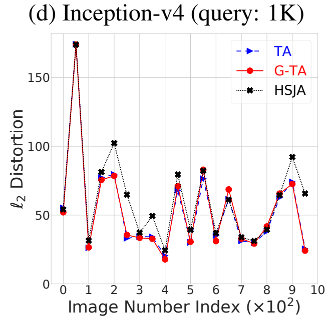

(g) SENet-154 (query: 1K)

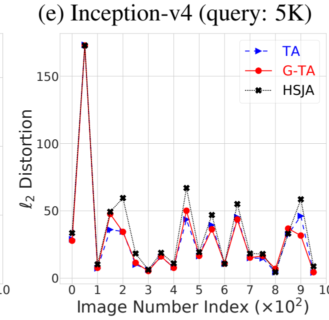

(h) SENet-154 (query: 5K)

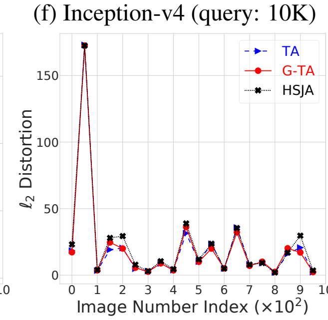

(i) SENet-154 (query: 10K)

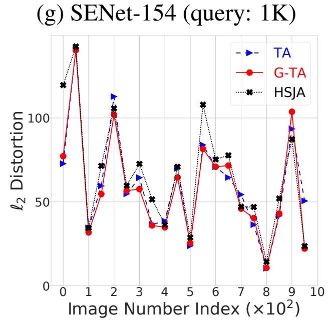

(j) ResNet-101 (query: 1K)

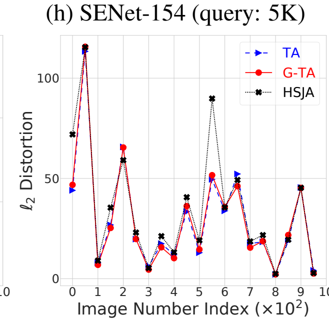

(k) ResNet-101 (query: 5K)

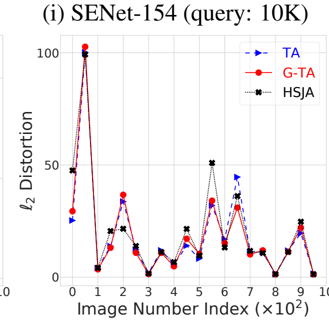

(l) ResNet-101 (query: 10K)

Figure 7: Comparisons of ℓ_2 distortions across 20 adversarial examples in targeted attacks of the ImageNet dataset.

D.4 Experimental Results of Median Distortions

In this section, we report the median ℓ_2 distortions of different query budgets on the CIFAR-10 and ImageNet datasets. Tables 8 and 9 show the experimental results. We can draw the following conclusions based on the results.

Table 8: Median ℓ_2 distortions of different query budgets on the ImageNet dataset. "-" denotes no adversarial example is found in this query budget.

Target Model	Method	Targeted Attack						Untargeted Attack					
		@300	@1K	@2K	@5K	@8K	@10K	@300	@1K	@2K	@5K	@8K	@10K
Inception-v3	BA [1]	105.513	101.877	101.056	97.481	81.269	73.524	-	109.507	103.637	96.340	79.027	58.924
	Sign-OPT [3]	96.905	83.215	66.601	43.350	31.036	25.380	115.140	73.319	38.327	12.761	8.277	6.808
	SVM-OPT [3]	**93.649**	77.838	63.631	42.897	31.838	26.322	114.879	59.343	**30.627**	12.085	8.352	7.025
	HSJA [2]	106.341	92.114	79.225	47.469	30.624	23.838	105.702	53.880	32.684	12.360	7.829	6.227
	TA	96.612	75.610	62.573	**38.226**	**25.892**	**19.993**	**95.302**	**50.878**	31.833	11.921	**7.464**	**6.030**
	G-TA	97.449	**75.499**	**62.484**	38.886	26.004	20.091	96.410	50.985	31.176	**11.861**	7.549	6.087
Inception-v4	BA [1]	104.275	101.115	99.872	96.700	79.412	71.387	-	116.855	112.335	104.557	85.044	64.123
	Sign-OPT [3]	95.388	81.865	66.159	42.871	31.241	25.798	121.725	77.838	40.465	14.268	8.924	7.153
	SVM-OPT [3]	**92.640**	77.616	62.949	42.552	31.142	26.238	120.407	64.600	**33.960**	**13.586**	9.035	7.535
	HSJA [2]	104.969	90.371	78.103	47.340	31.404	24.270	109.422	60.356	37.302	14.191	8.790	6.934
	TA	96.808	**74.829**	**61.974**	**37.155**	**26.128**	21.184	**101.170**	**55.876**	36.403	14.176	**8.592**	**6.814**
	G-TA	95.563	75.889	62.404	38.457	26.495	**21.069**	101.186	57.672	36.743	13.999	8.694	6.856
SENet-154	BA [1]	75.653	72.327	71.420	68.293	52.332	44.391	-	75.355	70.498	65.186	51.950	38.164
	Sign-OPT [3]	70.500	59.556	45.566	27.062	18.218	14.400	65.524	42.690	23.688	9.054	5.331	4.194
	SVM-OPT [3]	73.344	55.891	44.195	27.826	19.544	15.883	65.957	35.596	**20.549**	8.760	5.368	4.332
	HSJA [2]	72.589	60.361	49.487	25.718	14.929	12.197	70.043	34.697	21.811	8.098	4.482	3.707
	TA	66.285	**51.012**	**40.475**	**21.590**	**13.293**	**10.782**	**64.784**	34.034	22.269	**7.636**	4.273	3.555
	G-TA	**66.077**	51.852	41.065	21.946	13.461	10.899	65.122	**33.841**	21.823	7.772	**4.231**	**3.489**
ResNet-101	BA [1]	76.772	72.674	71.761	68.231	54.847	47.785	-	63.568	59.384	55.402	42.777	29.097
	Sign-OPT [3]	72.361	62.383	48.664	30.089	20.752	16.478	53.757	35.070	19.035	8.442	5.929	4.999
	SVM-OPT [3]	73.758	58.716	47.496	30.443	21.502	17.535	52.471	29.225	16.469	8.245	6.043	5.259
	HSJA [2]	73.422	60.175	49.443	26.504	16.035	12.661	54.869	24.971	15.161	6.084	3.787	3.237
	TA	69.511	**55.389**	44.343	24.500	**14.778**	**11.802**	**51.829**	24.748	15.162	5.941	**3.698**	3.203
	G-TA	**69.117**	56.275	**44.315**	**24.316**	15.133	11.946	51.883	**24.403**	**14.643**	**5.842**	3.703	**3.191**

Table 9: Median ℓ_2 distortions of different query budgets on the CIFAR-10 dataset.

Target Model	Method	Targeted Attack						Untargeted Attack					
-		300	@1K	@2K	@5K	@8K	@10K	300	@1K	@2K	@5K	@8K	@10K
PyramidNet-272	BA [1]	8.240	7.711	7.697	6.013	3.938	3.068	-	5.133	4.268	4.060	2.471	1.460
	Sign-OPT [3]	7.900	6.050	3.796	1.441	0.762	0.549	3.821	1.952	0.980	0.345	0.232	**0.196**
	SVM-OPT [3]	8.870	6.432	4.199	1.651	0.894	0.655	3.777	1.956	0.877	0.363	0.235	0.202
	HSJA [2]	7.616	4.013	2.109	**0.589**	0.384	0.325	3.935	**1.022**	**0.587**	0.294	0.224	0.201
	TA	7.650	**3.874**	**2.071**	0.599	**0.380**	**0.318**	**3.758**	1.028	0.589	0.289	**0.223**	0.197
	G-TA	**7.452**	3.980	2.110	0.602	0.387	0.324	3.938	1.033	0.590	**0.288**	0.224	0.198
GDAS	BA [1]	8.098	7.568	7.554	5.774	3.301	2.396	-	2.626	2.409	2.286	1.541	1.015
	Sign-OPT [3]	7.947	6.418	4.166	1.514	0.669	0.457	2.067	1.331	0.766	0.298	0.209	0.176
	SVM-OPT [3]	9.138	7.242	5.090	2.103	1.043	0.673	2.043	1.230	0.674	0.302	0.211	0.183
	HSJA [2]	7.687	3.061	1.383	0.435	0.298	0.254	1.905	0.674	0.429	0.232	0.185	0.168
	TA	**7.667**	**3.024**	**1.380**	0.435	**0.296**	**0.253**	1.932	0.690	**0.425**	0.228	0.185	0.169
	G-TA	7.728	3.104	1.385	**0.430**	0.298	**0.253**	**1.883**	**0.665**	0.428	**0.226**	**0.182**	**0.167**
WRN-28	BA [1]	8.317	7.789	7.764	5.493	2.199	1.293	-	3.900	3.332	3.167	1.361	0.732
	Sign-OPT [3]	7.737	5.188	2.816	0.797	0.439	0.354	2.679	1.298	0.723	0.281	**0.214**	**0.191**
	SVM-OPT [3]	9.054	5.697	3.317	0.981	0.511	0.398	2.627	1.279	0.627	0.288	0.218	0.198
	HSJA [2]	6.446	2.064	1.005	0.443	0.339	**0.306**	**2.497**	0.697	0.442	0.264	0.224	0.208
	TA	6.518	**2.018**	**0.988**	**0.428**	**0.337**	**0.306**	2.606	**0.682**	**0.431**	0.262	0.225	0.210
	G-TA	**6.444**	2.060	1.000	0.439	0.341	**0.306**	2.538	**0.682**	0.444	**0.261**	0.223	0.209
WRN-40	BA [1]	8.181	7.760	7.722	5.482	2.193	1.363	-	3.773	3.187	3.045	1.321	0.726
	Sign-OPT [3]	7.782	5.285	2.895	0.845	0.455	0.369	2.510	1.213	0.679	0.265	**0.194**	**0.173**
	SVM-OPT [3]	9.042	5.835	3.400	1.030	0.549	0.420	2.500	1.251	0.611	0.272	0.198	0.179
	HSJA [2]	6.578	2.183	1.040	0.439	0.338	**0.305**	2.470	0.702	0.453	0.256	0.214	0.198
	TA	6.747	2.100	**0.983**	**0.435**	**0.337**	**0.305**	2.584	**0.680**	**0.434**	**0.254**	0.215	0.201
	G-TA	**6.514**	**2.069**	1.014	0.438	0.339	0.306	**2.453**	0.695	0.441	0.255	0.213	0.199

(1) TA and G-TA perform better in attacking high-resolution images, *i.e.,* the images of the ImageNet dataset. The median ℓ_2 distortions of Table 8 are larger than that of Table 9, because the high-resolution images of the ImageNet dataset lead to larger ℓ_2 distortions.

(2) TA is more effective in the targeted attacks. We speculate that it is because the adversarial region of the target class is narrower and more scattered in the targeted attack, resulting in a smoother decision boundary. Thus, TA is more suitable for targeted attacks.

References

[1] Wieland Brendel, Jonas Rauber, and Matthias Bethge. Decision-based adversarial attacks: reliable attacks against black-box machine learning models. In *International Conference on Learning Representations*, pages 1–12, 2018.

[2] Jianbo Chen, Jordan Michael I., and Wainwright Martin J. HopSkipJumpAttack: a query-efficient decision-based adversarial attack. In *IEEE Symposium on Security and Privacy*, pages 1277–1294, 2020.

[3] Minhao Cheng, Simranjit Singh, Pin-Yu Chen, Sijia Liu, and Cho-Jui Hsieh. Sign-OPT: a query-efficient hard-label adversarial attack. In *International Conference on Learning Representations*, pages 1–16, 2020.

[4] Chuan Guo, Mayank Rana, Moustapha Cisse, and Laurens van der Maaten. Countering adversarial images using input transformations. In *International Conference on Learning Representations*, pages 1–12, 2018.

[5] Xiaojun Jia, Xingxing Wei, Xiaochun Cao, and Hassan Foroosh. ComDefend: an efficient image compression model to defend adversarial examples. In *IEEE/CVF Conference on Computer Vision and Pattern Recognition*, pages 6084–6092, 2019.

[6] Zihao Liu, Qi Liu, Tao Liu, Nuo Xu, Xue Lin, Yanzhi Wang, and Wujie Wen. Feature distillation: DNN-oriented jpeg compression against adversarial examples. In *IEEE/CVF Conference on Computer Vision and Pattern Recognition*, pages 860–868, 2019.

[7] Aleksander Madry, Aleksandar Makelov, Ludwig Schmidt, Dimitris Tsipras, and Adrian Vladu. Towards deep learning models resistant to adversarial attacks. In *International Conference on Learning Representations*, pages 1–28, 2018.

[8] Jonas Rauber, Wieland Brendel, and Matthias Bethge. Foolbox: a Python toolbox to benchmark the robustness of machine learning models. In *Reliable Machine Learning in the Wild Workshop of International Conference on Machine Learning*, pages 1–6, 2017.

[9] Jonas Rauber, Roland Zimmermann, Matthias Bethge, and Wieland Brendel. Foolbox Native: fast adversarial attacks to benchmark the robustness of machine learning models in PyTorch, TensorFlow, and JAX. *Journal of Open Source Software*, 5(53):2607, 2020.

[10] Haichao Zhang and Jianyu Wang. Defense against adversarial attacks using feature scattering-based adversarial training. In *Advances in Neural Information Processing Systems*, pages 1829–1839, 2019.

[11] Hongyang Zhang, Yaodong Yu, Jiantao Jiao, Eric Xing, Laurent El Ghaoui, and Michael Jordan. Theoretically principled trade-off between robustness and accuracy. In *International Conference on Machine Learning*, pages 7472–7482, 2019.